Synthesis of Cu/TiO_2 catalysts by reactive magnetron sputtering deposition and its application for photocatalytic reduction of CO_2 and H_2O to CH_4

Okorn Mekasuwandumrong[1], Nantiya Jantarasorn[2], Joongjai Panpranot[2], Marina Ratova[3], Peter Kelly[3] and Piyasan Praserthdam[2],*

[1] *Department of Chemical Engineering, Faculty of Engineering and Industrial Technology, Silpakorn University, Nakorn Pathom 73000, Thailand*

[2] *Center of Excellence on Catalysis and Catalytic Reaction, Department of Chemical Engineering, Faculty of Engineering, Chulalongkorn University, Bangkok, 10330, Thailand*

[3] *Surface Engineering Group, Faculty of Science and Engineering, Manchester Metropolitan University, Manchester, M1 5GD, United Kingdom*

Abstract

In the present work, a series of Cu/TiO_2 catalysts were successfully synthesized by using pulsed direct current (DC) reactive magnetron sputtering of Cu targets under Ar atmosphere onto various TiO_2 supports. The physiochemical properties of the catalysts were characterized by using inductive coupled plasma spectroscopy (ICP), X-ray diffraction (XRD), UV-Vis spectroscopy, N_2 physisorption, transmission electron microscopy (TEM), PL spectroscopy, and X-ray photoelectron spectroscopy (XPS). The photocatalytic activities of all the catalysts were studied via the photocatalytic reduction of CO_2 and H_2O to CH_4 under UV light irradiation. The Cu/TiO_2 catalysts exhibited higher photocatalytic activity than the uncoated TiO_2 supports and the ones made using an impregnation technique. The electron trapping of copper species, which prolonged the electron-hole recombination process, promoted photocatalytic activity of the Cu-doped catalysts. Moreover, the specific morphologies of the Cu species deposited on TiO_2 supports and the smaller change of bandgap energy of the sputter coated catalysts also resulted in an improvement of photocatalytic activity under UV light irradiation.

Keywords: photocatalytic; CO_2 reduction; Cu/TiO_2; methane; magnetron sputtering

1. Introduction

Presently, climate change and global warming are among the most serious environmental issues. The increase of atmospheric greenhouse gas concentration is widely considered as the main driving factor. Emission of CO_2 has the greatest impact on global warming, due to its relatively high emission to the atmosphere compared to other greenhouse gases [1, 2] . The main contributors of CO_2 emission are from power production, combustion of industrial fuels, construction, agriculture, and transportation. The solution to the problems is to reduce the release of CO_2 gas into the atmosphere or to convert it into other usable products. CO_2 can be used to generate valuable products, including methane, polycarbonate, methanol, acetic acid, formaldehyde, etc. [3-5] .

Photocatalytic reduction of CO_2 is an interesting process to convert CO_2 to various products such as carbon monoxide (CO) [6], methane (CH_4) [7], methanol (CH_3OH) [8], formic acid (HCOOH) [9], and formaldehyde (HCHO) [10]. With this technology, CO_2 is reduced with water as a reducing agent with UV light irradiation at room temperature and atmospheric pressure [11]. This process is relatively low cost, environmental friendly, and does not require thermal energy. Many photocatalysts have been attentively studied in this reaction [12]. Among those, TiO_2 is used most extensively due to its high stability, high photosensitivity, non-toxic nature, wide availability, and low cost [13]. However, TiO_2 has a high electron-hole pair recombination rates and weak CO_2 adsorption, which leads to low photocatalytic activity[14].

In order to improve the efficiency of TiO_2 in photocatalytic CO_2 reduction, it is necessary to increase the lifetime of the photogenerated electrons and holes via effective charge carrier separation and retardation of electron-hole recombination rate [15]. To accomplish this goal,

many methods have been proposed. It is well known that the structure and morphology of photocatalysts materials are critical to their photocatalytic performances [16-19]. Therefore, the effect of morphologies on the photocatalysts materials has been extensively studied. Doping TiO_2 with many kinds of metal/non-metal such as Cu[20], Pt[21], Au[22], Ag[23], and B[24] can also improve the photocatalytic efficiency of TiO_2. In a number of previous studies, deposition of Cu nanoparticles onto TiO_2 surface has been found to improve the photocatalytic efficiency of TiO_2 by altering the bandgap and preventing the recombination of photogenerated electron-hole pairs, which showed effectiveness in CO_2 photoreduction [25]. Besides, Cu nanoparticles were selected due to their high yield of methane formation [7, 26].

In general, the preparation of metal doped TiO_2 catalysts is mostly done by conventional impregnation method, which usually requires a metal precursor solution and heat treatment, which generates waste. Reactive magnetron sputtering is a commercial process to prepare a thin film product for various applications ranging from solar glazing products to micro-electronic coatings, from tool protecting layers to packaging coatings [27]. Applying this method to prepare powder products can offer a new direct metal deposition method on a powder support, which can be carried out in a one-step process without generation of waste [28].

In this work, we present the results of the deposition of Cu clusters on various TiO_2 supports by using the pulsed magnetron sputtering technique and compare these samples with the ones prepared by a conventional impregnation method. The physiochemical properties of the obtained-catalysts were characterized and their photocatalytic properties were tested in the photocatalytic reduction of CO_2 and H_2O to CH_4.

2. Experimental

2.1 Catalytic preparation

The Cu/TiO_2 catalysts were prepared by using the pulsed magnetron sputtering method to deposit Cu on various TiO_2 supports. Three types of TiO_2 including P25, pure anatase TiO_2 and pure rutile TiO_2 were used as the catalyst supports. 2 g of each TiO_2 support was loaded in the sputtering chamber. The TiO_2 powder was placed in an oscillating bowl positioned directly underneath the 75 mm diameter Cu sputtering target. The oscillator caused the powder particles to move around the bowl during the deposition process and, therefore, resulted in a uniform coating on the substrate. The synthesis conditions including power; 200W and pulse frequency (F); 200 kHz were used. The pulsed magnetron sputtering of the Cu target was done in an argon atmosphere at 2 Pa. The sputtering time was varied at 2.5, 5, and 7.5 min.

For comparison purposes, Cu/TiO_2 catalysts were also prepared by the conventional incipient wetness impregnation method. Approximately 2 g of TiO_2 was doped with an aqueous solution of copper (II) nitrate trihydrate ($Cu(NO_3)_2 \cdot 3H_2O$). The metal precursor solution was slowly dropped onto the TiO_2 supports to obtain the desired content. The obtained sample was dried in an oven at 110°C overnight and then calcined in a box furnace at 400°C under an air flow with a heating rate 10°C/min and held at that temperature for 2 h.

2.2 Catalyst characterization

The crystal structures of catalyst particles were examined by powder X-ray diffraction (XRD) using a SIEMENS XRD D5000 X-ray diffractometer with CuK_α radiation. The scans

were recorded over a range of 2θ angles from 10º to 80º. The average crystallite size of the catalysts was calculated from line broadening according to Scherrer′s equation. The amount of Cu loading in catalysts were measured by Inductively Coupled Plasma- Optical Emission Spectroscopy (ICP- OES) using Perkin Elmer Optima 7000DV. The BET surface area was obtained from the nitrogen adsorption isotherm at 77 K using a BEL-SORP automated system. The band gap energy of catalysts was determined by UV-Vis spectrometer using LAMDA 650 UV/Vis spectrophotometer to study in electronic properties. The morphologies of the Cu/TiO_2 catalysts were determined by transmission electron microscope (TEM) using a JEOL- JEM 2010 transmission electron microscope using energy- dispersive X- ray detector operated at 200kV. The surface properties was determined by using X- ray photoelectron spectroscopy (XPS) using ANICUS photoelectron spectrometer equipped with a Mg Kα that X- ray as a primary excitation and a KRATOS VISION 2 software. The photoluminescence spectroscopy (PL) was examined using Fluromax® by Horiba and using Xenon lamp source excitation at 320 nm. The thermogravimetric analysis was examined with air by using SDT Q600 V8.3 Build 101.

2.3 Photocatalytic reaction

The photocatalytic reductions of CO_2 with water were carried out in a photoreactor system. Six UV-light bulbs were installed around a cylindrical quartz reactor. 0.5 g of catalyst was dispersed into a stirred slurry reactor (SSR), which contained 150 mL of deionized water. Prior to the reaction test, compressed CO_2 (>99.99 %) was flowed into the system from an inlet

tube in the cylindrical quartz reactor with a flow rate of 100 ml/ min using a mass flow controller for 30 min. to eliminate other gases and saturate the solution. During the reaction, the reactor is closed and a magnetic stirrer agitated the catalyst-suspended solution throughout the experiment. The photocatalytic reaction was started by turned on the UV light, and irradiation was continued for 6 h. The resultant gas samples were analyzed using a two GC-14B (Shimadzu) gas chromatographs equipped with a flame ionization detector (FID) and thermal conductivity detector for hydrocarbon and other gases analysis. The photocatalytic reaction was performed for 2 h and the methane production yield can be calculated according to the following equation:

$$CH_4 \text{ production yield} = \frac{\text{Total amount of } CH_4 \text{ evolved per g of catalyst } (\mu\text{mol. gcat}^{-1})}{\text{Reaction time (h)}}$$

The quantum efficiencies of the photocatalysts were measured under the same photocatalytic reaction conditions. The light intensity was estimated using a research radiometer (MODE IL-1700). The QE for CO_2 reduction to CH_4 was calculated using the following equation:

$$\text{QE (\%)} = \frac{\text{number of reacted electrons}}{\text{number of incident photons}} \times 100$$

$$\text{QE (\%)} = \frac{8 \text{ x number of evolved } CH_4 \text{ molecules}}{\text{number of incident photons}} \times 100$$

3. Results and discussion

3.1 Characterization of the sputtered Cu/TiO_2 catalysts

The XRD patterns of all the sputtered- and the impregnation-made catalysts are shown in Figure 1. Both sputtered- and impregnation-made Cu deposited on P25 and anatase TiO_2 catalysts exhibited the main characteristic peaks of the anatase phase located at $2\theta = 25.3$ (101), 37.8 (004), 48.0 (200), 54.5, (105 and 211), and 62.8 (213). The additional peaks of the rutile phase were only observed for Cu supported on P25 catalysts at 2θ degrees = 27.5 (110). In the case of Cu deposited on rutile TiO_2, only the characteristic peaks of the rutile phase were observed. There were no additional peaks corresponding to Cu/CuO phases in all the sputterred- and impregnation-made catalysts. This is probably due to the low amount of Cu loading and/or high dispersion of Cu/CuO on the TiO_2 supports. The physical properties such as crystallite size, BET surface area and band gap energy of all the catalysts are summarized in Table 1. It can be seen that deposition of Cu by both methods did not affect the crystal structure, crystallite size, and BET surface area of the Cu/TiO_2 catalyst even after prolonging the sputtering time or increasing of Cu loading content.

The actual amount of Cu loading of all the sputtered-catalysts were measured by using ICP technique. A Plot showing the relationship between %Cu loading content and sputtering time is shown in Figure 2. The Cu contents increased linearly with sputtering time, due to the constant flux of Cu atoms deposited on the supports. The amount of Cu increased in the order of P25 > rutile > anatase. The differences in Cu loadings could be attributed to the different powder distribution patterns in the oscillating bowl. In order to compare the Cu/TiO_2 catalysts

prepared by different methods, the catalysts with similar %Cu loading content were also prepared by impregnation and the ICP results are summarized in Table 1.

The UV-Vis absorption spectra of the sputtered catalysts are shown in Figure 3. Typical absorption spectra of Cu modified TiO_2 materials consisted of three main characteristic bands, including the sharp absorption band at wavelengths less than 400 nm, which were attributed to the band structure of the original TiO_2, the absorption band at wavelengths of 700–800 nm, due to the Cu d-d transition, and an absorption tail in the 400–500 nm region, which was attributed to the interfacial charge transfer (IFCT) phenomenon between TiO_2 valence band electrons and Cu(II) species. The impregnation-made catalysts exhibited all three adsorption bands and the peak intensity increased with increasing of Cu loading content, indicating the formation of Cu nanoparticles and the interaction between Cu (II) species and the TiO_2 support. On the other hand, the sputtered catalysts exhibited typical adsorption bands of the TiO_2 and Cu nanoparticles but the absorption tail between 400 and 500 nm related to IFCT was absent or much less apparent.

The band gap energy of all the Cu/TiO_2 samples were determined from the extrapolation of Tauc plots of $(h\nu\alpha)^{1/2}$ as a function of photon energy $(h\nu)$ and the obtained results are shown in Table 1. For the impregnation-made catalysts, the band gap of the TiO_2 supports shifted towards longer wavelengths after doping with Cu. However, in the case of the sputtered catalysts, only a small shift was observed. This indicates that there was less interaction between the Cu and the TiO_2 supports when prepared by the sputtering method. The differences in the interaction between the sputtered coating and the support could be attributed to the different temperatures used in the deposition process. In the impregnation process, the

catalysts were subjected to heat treatment at 400ºC in order to decompose the Cu precursors and form CuO, while the sputtering process can be done at room temperature in vacuum. As a consequence, the main structural characteristics of the supporting powder remained unaltered.

The morphology of all the Cu/TiO_2 catalysts was determined by transmission electron microscopy. Typical TEM images of the Cu/TiO_2 catalysts are presented in Figure 4. The catalysts made via the sputtering process exhibited an irregular shape with well-dispersed Cu particles of a size around 2 to 6 nm. The irregular metal particles were the specific structure of the deposited metal prepared by using the pulsed magnetron sputtering process [29-31] whereas the impregnation-made catalysts exhibited spherical Cu clusters deposited on the TiO_2 supports.

Photoluminescence spectroscopy is used to investigate the efficiency of charge carrier trapping, immigration and transfer in a photocatalysts. Figure 5 shows the PL spectra of all Cu/TiO_2 catalysts. There are many PL peaks can be detected in the visible region. The peak at 436 nm corresponded to the self-trapped electron localized on TiO_6[32] and the peaks at 469, 484, 492 nm corresponded to the oxygen vacancies with two trapped electrons on TiO_2 surface[33, 34]. From our results, the PL spectra decreased as the Cu loading content increased for both preparation methods except for the impregnation-made Cu supported on rutile TiO_2 support in which doping with Cu resulted in an increase of PL signal (except IM2-Rut). PL spectroscopy measures the energy release during the electron-hole recombination process, therefore decrease of photoluminescence energy suggests the reduction of recombination rate. Decreasing of the PL signal after doping with Cu was attributed to the trapping of photoelectron

from the conduction band of TiO_2 by Cu^{2+}, which could slow down the electron-hole recombination process.

XPS was used to investigate the surface properties of each element in the obtained Cu/TiO_2 catalysts. The XPS spectra of Ti 2p, O 1s and Cu 2p of all Cu/TiO_2 catalysts are shown in Figure 6. Generally, the binding energies corresponding to Ti $2p_{1/2}$ and Ti $2p_{3/2}$ in pure TiO_2 were located at around 465 and 459 eV, respectively. These peaks corresponded to the Ti^{4+} valence state on lattice oxygen[35-37]. The two shoulder peaks centered at 463 and 457.3 eV could be assigned to Ti_2O_3 corresponding with Ti^{3+} valence state[38, 39]. The characteristic peaks of Ti 2p did not change after addition of copper by both preparation methods. Figure 6b shows the XPS spectra of the O 1s for the Cu/TiO_2 catalysts. Both catalysts showed main peaks and a shoulder centered at 530.7 and 532 eV, which were assigned to lattice oxide ions in TiO_2 and the hydroxyl groups on the TiO_2 surface, respectively[40]. The characteristic peaks of Cu $2p_{3/2}$ and Cu $2p_{1/2}$ peaks of the prepared catalysts by both methods were located around 933.6-934.2 eV and 953.1-954.9 eV, respectively. The satellite peak also presented at 944 eV. These peaks were consistent with those of the Cu^{2+} cations[41]. A small shift to higher binding energies (1 eV) was observed from impregnation-made catalyst, suggesting the different interaction between Cu and TiO_2 support.

3.2 Photocatalytic activity

The photocatalytic activity of all the Cu/TiO_2 catalysts were evaluated by the photocatalytic reduction of CO_2 in water at ambient temperature under UV-light irradiation.

The control experiment showed that there were no hydrocarbon products in the absence of photocatalysts or UV light irradiation. This suggests that the hydrocarbon product can be produced only by photocatalytic reaction using photocatalysts. From our test results, methane was the main product obtained from all the Cu/TiO_2 catalysts. Figure 7 shows the graph of the CH_4 production yield of all the samples. Among the three TiO_2 supports, rutile TiO_2 exhibited the highest CH_4 production yield. Deposition of Cu by magnetron sputtering on the TiO_2 support increased the CH_4 production yield. Loading small amounts of Cu by the impregnation method also improved the CH_4 production yield, however, further increase of Cu doping content, the CH_4 production yield for all the TiO_2 supports decreased. Quantum efficiency of the photocatalytic CO_2 reduction of all catalysts have also been calculated and reported in Table 2. The % quantum efficiency was calculated to be in the range of 0.08 to 0.74%.

Improvement of the photocatalytic efficiency of TiO_2 after Cu deposition can be explained by the reduction of the probability of photoexcited e^- and hole h^+ recombination due to the electron trapping of Cu clusters. However, in the case of impregnation-made catalysts, increasing the Cu loading content also reduced band gap energy, which made energy level between the conduction and valence bands became narrower and promoted the electron hole recombination. Whilst, in the case of sputtered catalysts, the band gap energy did not change much, therefore, it was beneficial for the trapping process without the penalty from narrowing the band gap. Moreover, increasing of Cu loading on TiO_2 surface also resulted in the coverage of Cu species on TiO_2 surface, which could block the light on TiO_2 surface.

In order to investigate the stability and the recyclability of the prepared catalysts, the photocatalytic CO_2 reduction performances of the Cu deposited on P25-TiO_2 catalysts prepared by both methods were determined repeatedly for three consecutive batches. The used catalysts

were recovered by using centrifugal and filtration from the obtained reaction mixture and then were re-used. Figure 8 shows the plot of CH_4 production yield obtained from various cycles. The CH_4 production yield was found to be quite stable with negligible loss (less than 15%). Such results suggest that the prepared Cu/ TiO_2 catalyst can be reused for a long-term application.

Conclusions

Reactive magnetron sputtering was used to deposit Cu clusters on various TiO_2 supports. The Cu loading content increased linearly with increasing sputtering time due to the constant Cu flux in the sputtering process. Irregular shaped Cu clusters were observed on the catalysts produced by sputtering, whereas spherical clusters were mainly obtained by impregnation. The UV-Vis spectra results revealed that increasing the Cu deposition content by magnetron sputtering slightly decreased the band gap energy whereas impregnation method led to a significant change in the band gap energy due to the different interactions between the Cu species and the TiO_2 supports. The sputtered Cu/ TiO_2 catalysts exhibited higher photocatalytic activity than the undoped TiO_2 supports and the impregnation-made ones. The electron trapping of copper species, which prolonged the electron-hole recombination process, promoted photocatalytic activity of the Cu-doped catalysts with a little change in the band gap energy.

Acknowledgments:

This research is supported by Newton Mobility Grants and Malaysia-Thailand Joint Authority Research Cess Fund Project.

References

[1] I.-H. Tseng, W.-C. Chang, J.C. Wu, Photoreduction of CO_2 using sol–gel derived titania and titania-supported copper catalysts, Applied Catalysis B: Environmental, 37 (2002) 37-48.

[2] K. Kočí, L. Obalová, L. Matějová, D. Plachá, Z. Lacný, J. Jirkovský, O. Šolcová, Effect of TiO_2 particle size on the photocatalytic reduction of CO_2, Applied Catalysis B: Environmental, 89 (2009) 494-502.

[3] Q. Li, L. Zong, C. Li, J. Yang, Reprint of "Photocatalytic reduction of CO_2 on MgO/TiO_2 nanotube films", Applied Surface Science, 319 (2014) 16-20.

[4] W. Qingli, Z. Zhaoguo, C. Xudong, H. Zhengfeng, D. Peimei, C. Yi, Z. Xiwen, Photoreduction of CO_2 using black TiO_2 films under solar light, Journal of CO_2 Utilization, 12 (2015) 7-11.

[5] W.A. Thompson, C. Perier, M.M. Maroto-Valer, Systematic study of sol-gel parameters on TiO_2 coating for CO_2 photoreduction, Applied Catalysis B: Environmental, 238 (2018) 136-146.

[6] Z. Xiong, H. Wang, N. Xu, H. Li, B. Fang, Y. Zhao, J. Zhang, C. Zheng, Photocatalytic reduction of CO_2 on Pt^{2+}–Pt^0/TiO_2 nanoparticles under UV/Vis light irradiation: a combination of Pt^{2+} doping and Pt nanoparticles deposition, International journal of hydrogen energy, 40 (2015) 10049-10062.

[7] Z. Xiong, Z. Lei, C.-C. Kuang, X. Chen, B. Gong, Y. Zhao, J. Zhang, C. Zheng, J.C. Wu, Selective photocatalytic reduction of CO_2 into CH_4 over Pt-Cu_2O TiO_2 nanocrystals: the interaction between Pt and Cu_2O cocatalysts, Applied Catalysis B: Environmental, 202 (2017) 695-703.

[8] M. Anpo, H. Yamashita, Y. Ichihashi, Y. Fujii, M. Honda, Photocatalytic reduction of CO_2 with H_2O on titanium oxides anchored within micropores of zeolites: effects of the structure of the active sites and the addition of Pt, The Journal of Physical Chemistry B, 101 (1997) 2632-2636.

[9] S. Sato, T. Morikawa, S. Saeki, T. Kajino, T. Motohiro, Visible-light-induced selective CO_2 reduction utilizing a ruthenium complex electrocatalyst linked to ap-type nitrogen-doped Ta_2O_5 semiconductor, Angewandte Chemie, 122 (2010) 5227-5231.

[10] T. Inoue, A. Fujishima, S. Konishi, K. Honda, Photoelectrocatalytic reduction of carbon dioxide in aqueous suspensions of semiconductor powders, Nature, 277 (1979) 637-638.

[11] D. Liu, Y. Fernández, O. Ola, S. Mackintosh, M. Maroto-Valer, C.M. Parlett, A.F. Lee, J.C. Wu, On the impact of Cu dispersion on CO_2 photoreduction over Cu/TiO_2, Catalysis Communications, 25 (2012) 78-82.

[12] S. Das, W.W. Daud, A review on advances in photocatalysts towards CO_2 conversion, Rsc Advances, 4 (2014) 20856-20893.

[13] S. Krejčíková, L. Matějová, K. Kočí, L. Obalová, Z. Matěj, L. Čapek, O. Šolcová, Preparation and characterization of Ag- doped crystalline titania for photocatalysis applications, Applied Catalysis B: Environmental, 111 (2012) 119-125.

[14] O. Ola, M.M. Maroto-Valer, Review of material design and reactor engineering on TiO2 photocatalysis for CO_2 reduction, Journal of Photochemistry and Photobiology C: Photochemistry Reviews, 24 (2015) 16-42.

[15] J. Low, B. Cheng, J. Yu, Surface modification and enhanced photocatalytic CO_2 reduction performance of TiO_2: a review, Applied Surface Science, 392 (2017) 658-686.

[16] Y. Li, X. Deng, J. Tian, Z. Liang, H. Cui, Ti_3C_2 MXene-derived Ti_3C_2/TiO_2 nanoflowers for noble-metal-free photocatalytic overall water splitting, Applied Materials Today, 13 (2018) 217-227.

[17] B. Sun, Y. Qian, Z. Liang, Y. Guo, Y. Xue, J. Tian, H. Cui, Oxygen vacancy-rich BiO_{2-x} ultra-thin nanosheet for efficient full-spectrum responsive photocatalytic oxygen evolution from water splitting, Solar Energy Materials and Solar Cells, 195 (2019) 309-317.

[18] B. Yin, C. Liu, Convenient Synthesis and Enhanced Photocatalytic Activity of BiOI/ BiOBr Nanostructures with Different Morphologies, Journal of nanoscience and nanotechnology, 18 (2018) 4771-4779.

[19] Y. Li, T. Li, J. Tian, X. Wang, H. Cui, TiO_2 Nanobelts Decorated with In_2S_3 Nanoparticles as Photocatalysts with Enhanced Full□Solar□Spectrum (UV–vis–NIR) Photocatalytic Activity toward the Degradation of Tetracycline, Particle & Particle Systems Characterization, 34 (2017) 1700127.

[20] H.W. Nasution, E. Purnama, S. Kosela, J. Gunlazuardi, Photocatalytic reduction of CO_2 on copper-doped Titania catalysts prepared by improved-impregnation method, Catalysis Communications, 6 (2005) 313-319.

[21] W.-N. Wang, W.-J. An, B. Ramalingam, S. Mukherjee, D.M. Niedzwiedzki, S. Gangopadhyay, P. Biswas, Size and structure matter: enhanced CO_2 photoreduction efficiency by size-resolved ultrafine Pt nanoparticles on TiO_2 single crystals, Journal of the American chemical society, 134 (2012) 11276-11281.

[22] S.t. Neaţu, J.A. Maciá-Agulló, P. Concepción, H. Garcia, Gold–copper nanoalloys supported on TiO_2 as photocatalysts for CO_2 reduction by water, Journal of the American Chemical Society, 136 (2014) 15969-15976.

[23] K. Kočí, K. Matějů, L. Obalová, S. Krejčíková, Z. Lacný, D. Plachá, L. Čapek, A. Hospodková, O. Šolcová, Effect of silver doping on the TiO_2 for photocatalytic reduction of CO2, Applied Catalysis B: Environmental, 96 (2010) 239-244.

[24] L. Shindume, Z. Zhao, N. Wang, H. Liu, A. Umar, J. Zhang, T. Wu, Z. Guo, Enhanced photocatalytic activity of B, N-codoped TiO_2 by a new molten nitrate process, Journal of Nanoscience and Nanotechnology, 19 (2019) 839-849.

[25] H. Yan, T. Zhao, X. Li, C. Hun, Synthesis of Cu-doped nano-TiO_2 by detonation method, Ceramics International, 41 (2015) 14204-14211.

[26] Y. Li, W.-N. Wang, Z. Zhan, M.-H. Woo, C.-Y. Wu, P. Biswas, Photocatalytic reduction of CO_2 with H_2O on mesoporous silica supported Cu/TiO_2 catalysts, Applied Catalysis B: Environmental, 100 (2010) 386-392.

[27] M. Ratova, R. Klaysri, P. Praserthdam, P.J. Kelly, Visible light active photocatalytic C-doped titanium dioxide films deposited via reactive pulsed DC magnetron co-sputtering: Properties and photocatalytic activity, Vacuum, 149 (2018) 214-224.

[28] Y. Zhang, H. Ma, M. Yi, Z. Shen, X. Yu, X. Zhang, Magnetron-sputtering fabrication of noble metal nanodots coated TiO_2 nanoparticles with enhanced photocatalytic performance, Materials & Design, 125 (2017) 94-99.

[29] H. Wang, Y. Li, X. Ba, L. Huang, Y. Yu, TiO_2 thin films with rutile phase prepared by DC magnetron co-sputtering at room temperature: effect of Cu incorporation, Applied Surface Science, 345 (2015) 49-56.

[30] L. Chen, M.E. Graham, G. Li, D.R. Gentner, N.M. Dimitrijevic, K.A. Gray, Photoreduction of CO_2 by TiO_2 nanocomposites synthesized through reactive direct current magnetron sputter deposition, Thin Solid Films, 517 (2009) 5641-5645.

[31] W. Hui, S. Guodong, Z. Xiaoshu, Z. Wei, H. Lin, Y. Ying, In-situ synthesis of TiO_2 rutile/anatase heterostructure by DC magnetron sputtering at room temperature and thickness effect of outermost rutile layer on photocatalysis, Journal of Environmental Sciences, 60 (2017) 33-42.

[32] H. Khan, D. Berk, Effect of a chelating agent on the physicochemical properties of TiO_2: characterization and photocatalytic activity, Catalysis letters, 144 (2014) 890-904.

[33] P. Verma, S.K. Samanta, Degradation kinetics of pollutants present in a simulated wastewater matrix using UV/TiO_2 photocatalysis and its microbiological toxicity assessment, Research on Chemical Intermediates, 43 (2017) 6317-6341.

[34] Y. Jiang, Z. Yang, P. Zhang, H. Jin, Y. Ding, Natural assembly of a ternary Ag−SnS−TiO_2 photocatalyst and its photocatalytic performance under simulated sunlight, RSC Advances, 8 (2018) 13408-13416.

[35] K. Imamura, S.-i. Iwasaki, T. Maeda, K. Hashimoto, B. Ohtani, H. Kominami, Photocatalytic reduction of nitrobenzenes to aminobenzenes in aqueous suspensions of titanium (IV) oxide in the presence of hole scavengers under deaerated and aerated conditions, Physical Chemistry Chemical Physics, 13 (2011) 5114-5119.

[36] R. Bhosale, R. Hyam, P. Dhanya, S. Ogale, Chlorate ion mediated rutile to anatase reverse phase transformation in the TiO_2 nanosystem, Dalton Transactions, 40 (2011) 11374-11377.

[37] K. Imamura, K. Hashimoto, H. Kominami, Chemoselective reduction of nitrobenzenes to aminobenzenes having reducible groups by a titanium (IV) oxide photocatalyst under gas-and metal-free conditions, Chemical Communications, 48 (2012) 4356-4358.

[38] N.R.F. Machado, V.S. Santana, Influence of thermal treatment on the structure and photocatalytic activity of TiO_2 P25, Catalysis Today, 107 (2005) 595-601.

[39] G. Wang, L. Xu, J. Zhang, T. Yin, D. Han, Enhanced photocatalytic activity of powders (P25) via calcination treatment, International Journal of Photoenergy, 2012 (2012).

[40] A. Naldoni, M. Allieta, S. Santangelo, M. Marelli, F. Fabbri, S. Cappelli, C.L. Bianchi, R. Psaro, V. Dal Santo, Effect of nature and location of defects on bandgap narrowing in black TiO_2 nanoparticles, Journal of the American Chemical Society, 134 (2012) 7600-7603.

[41] M.-K. Jeon, J.-W. Park, M. Kang, Hydrogen production from methanol/water decomposition in a liquid photosystem using the anatase and rutile forms of Cu-TiO_2, Journal of Industrial and Engineering Chemistry, 13 (2007) 84-91.

Table 1 Summary of the characteristic properties of Cu/TiO_2 catalysts

Catalyst	[a]Crystallite size (nm)		[b]Surface area	[c]band gap energy	[d]Wt% of Cu
	Anatase	Rutile	(m^2/g)	(eV)	
P25-TiO_2	20	23	54	3.21	-
SP1-P25	19	25	53	3.09	0.73
SP2-P25	18	24	54	3.04	1.44
SP3-P25	19	23	54	3.01	2.21
IM1-P25	18	22	51	2.96	0.68
IM2-P25	18	22	52	2.55	1.57
IM3-P25	17	21	52	2.53	2.47
Ana-TiO_2	20	-	111	3.23	-
SP1-Ana	18	-	110	3.21	0.33
SP2-Ana	20	-	110	3.2	0.65
SP3-Ana	19	-	106	3.16	1.18
IM1-Ana	17	-	80	3.14	0.34
IM2-Ana	19	-	81	3.01	0.70
IM3-Ana	18	-	79	2.83	1.40
Rut-TiO_2	-	23	171	3.17	-
SP1-Rut	-	21	169	3.14	0.52
SP2-Rut	-	17	170	3.09	1.18
SP3-Rut	-	15	169	3.06	1.91
IM1-Rut	-	19	144	2.83	0.57
IM2-Rut	-	20	143	2.75	1.23
IM3-Rut	-	18	142	2.68	2.11

[a] Average crystalline size was determined by XRD using Scherrer equation.

[b] The BET surface area was determined by single point BET method.

[c] band gap energy was calculated by UV-visible absorption spectra.

[d]Weight percent was determined by ICP.

Table 2 CH_4 production yield after 6 h of irradiation and formal % quantum efficiency (Q.E.) of all catalysts

Catalyst	CH_4 yields (μmole.gcat.h^{-1})	Q.E. (%)
P25-TiO_2	0.27	0.08
SP1-P25	1.25	0.39
SP2-P25	1.15	0.36
SP3-P25	1.86	0.59
IM1-P25	0.74	0.23
IM2-P25	1.45	0.46
IM3-P25	0.88	0.28
Ana-TiO_2	0.59	0.19
SP1-Ana	0.87	0.27
SP2-Ana	0.93	0.29
SP3-Ana	1.23	0.39
IM1-Ana	0.51	0.16
IM2-Ana	1.1	0.35
IM3-Ana	0.77	0.24
Rut-TiO_2	1.39	0.44
SP1-Rut	1.76	0.55
SP2-Rut	1.53	0.48
SP3-Rut	1.89	0.59
IM1-Rut	1.09	0.34
IM2-Rut	2.35	0.74
IM3-Rut	1.35	0.42

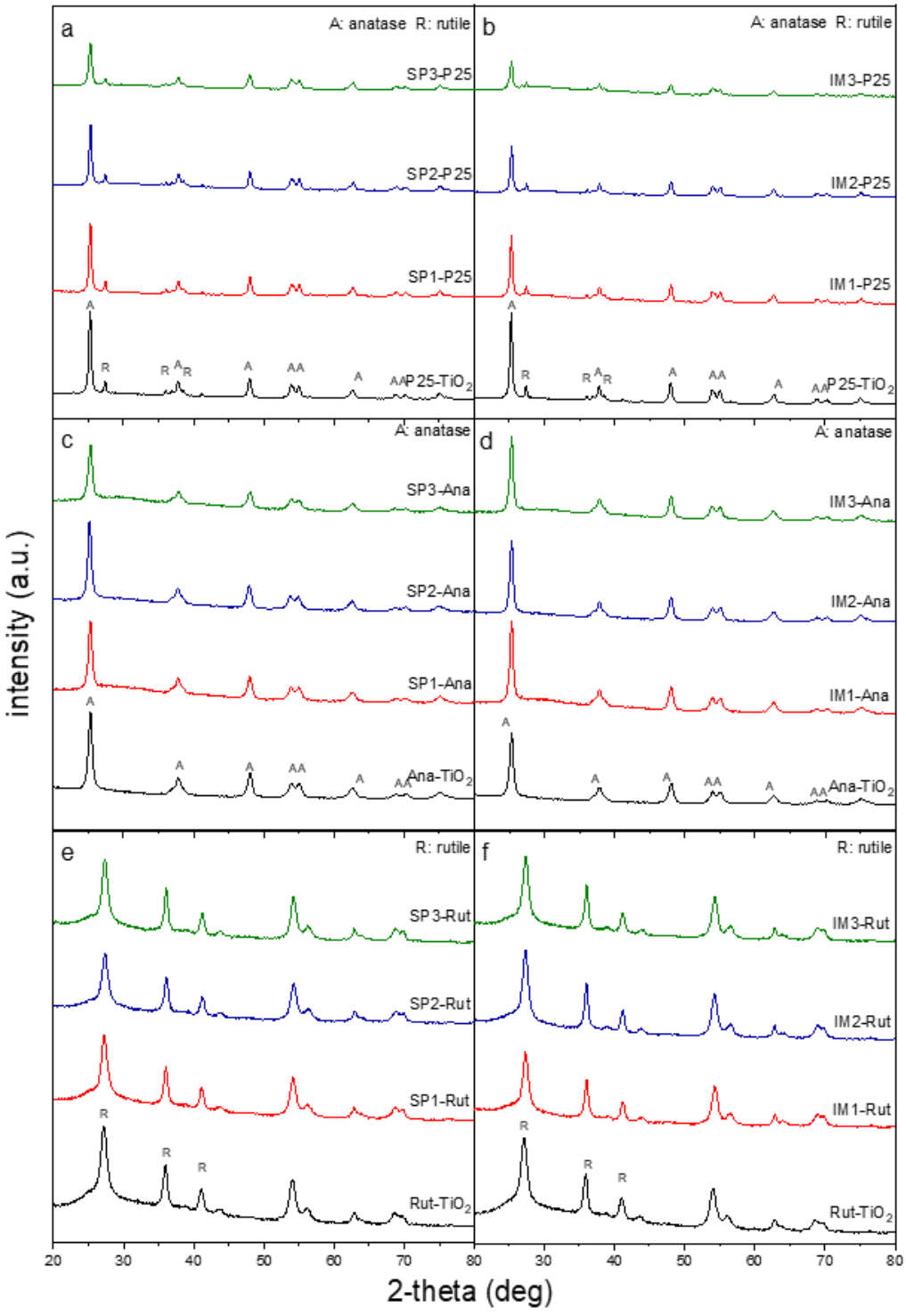

Figure 1 XRD patterns of P25, Ana and Rut modified with Cu nanoparticles prepared by magnetron sputtering (a,c,e) and incipient wetness impregnation (b,d,f) methods.

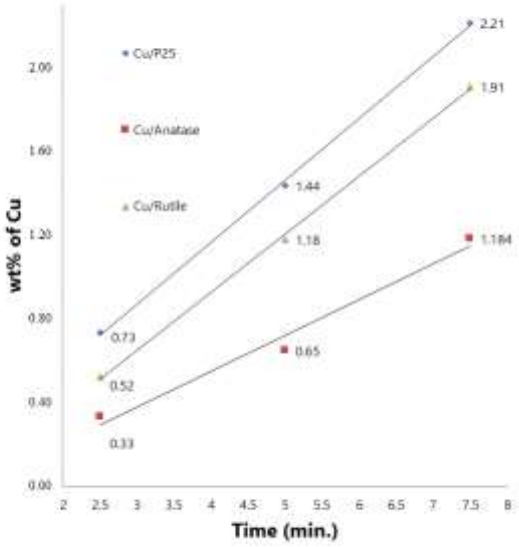

Figure 2. %Wt. of Cu-adhered onto P25-TiO_2, Ana-TiO_2, and Rut-TiO_2 supports prepared magnetron sputtering method.

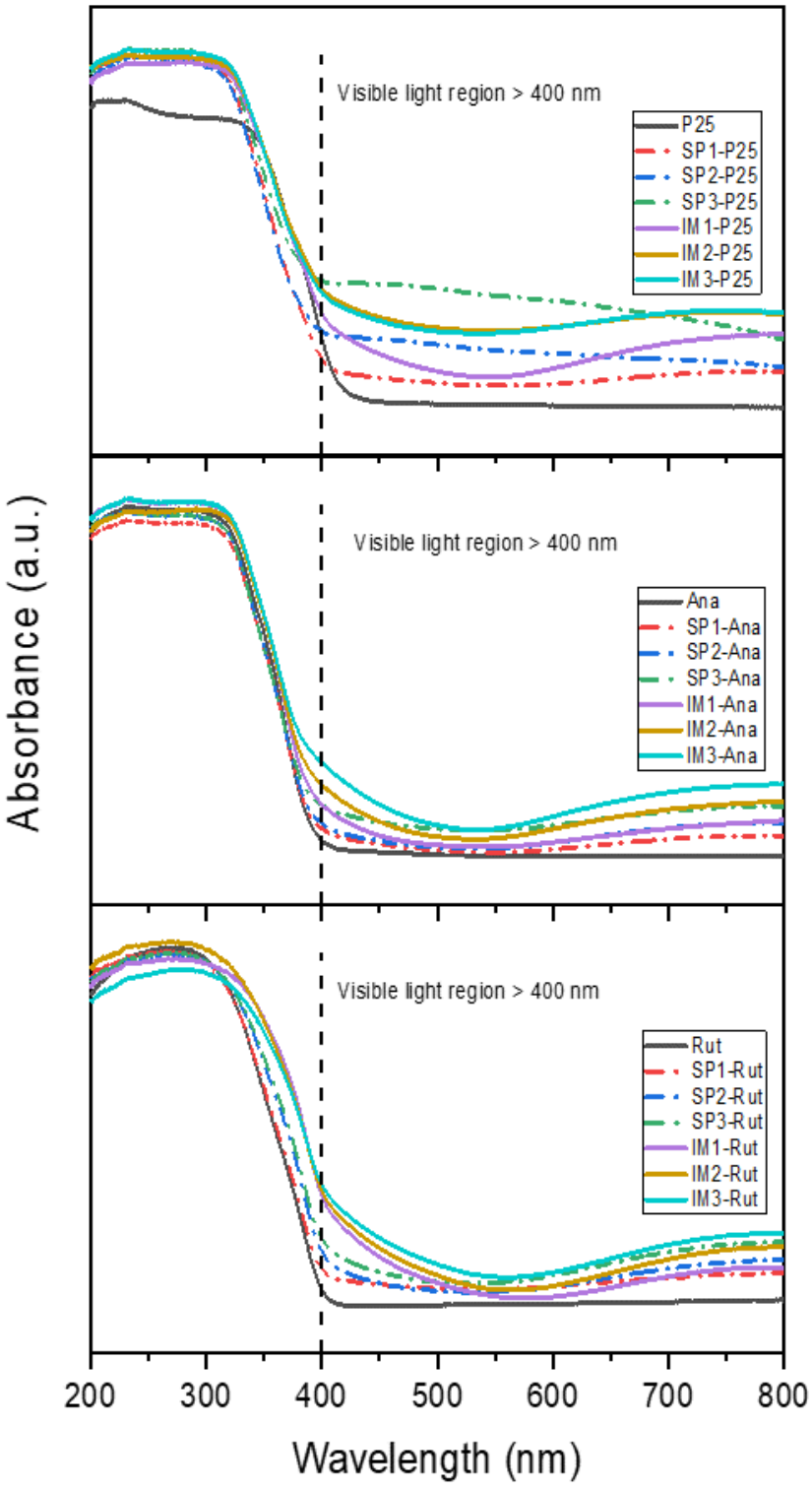

Figure 3. The UV-Vis absorption spectra of P25-TiO_2, Ana-TiO_2 and Rut-TiO_2 modified with Cu nanoparticles prepared by magnetron sputtering and incipient wetness impregnation methods.

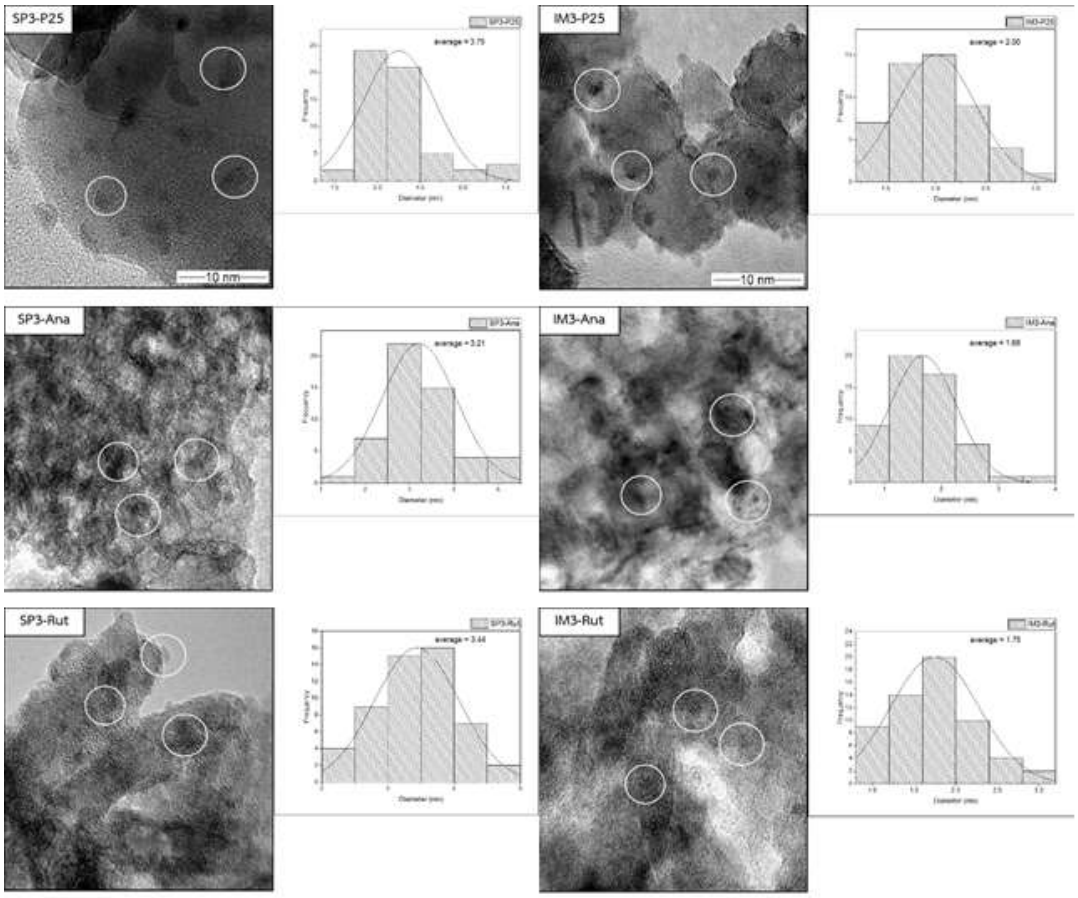

Figure 4.TEM images of P25-TiO_2, Ana-TiO_2 and Rut-TiO_2 modified Cu nanoparticles prepared by magnetron sputtering method and incipient wetness impregnation.

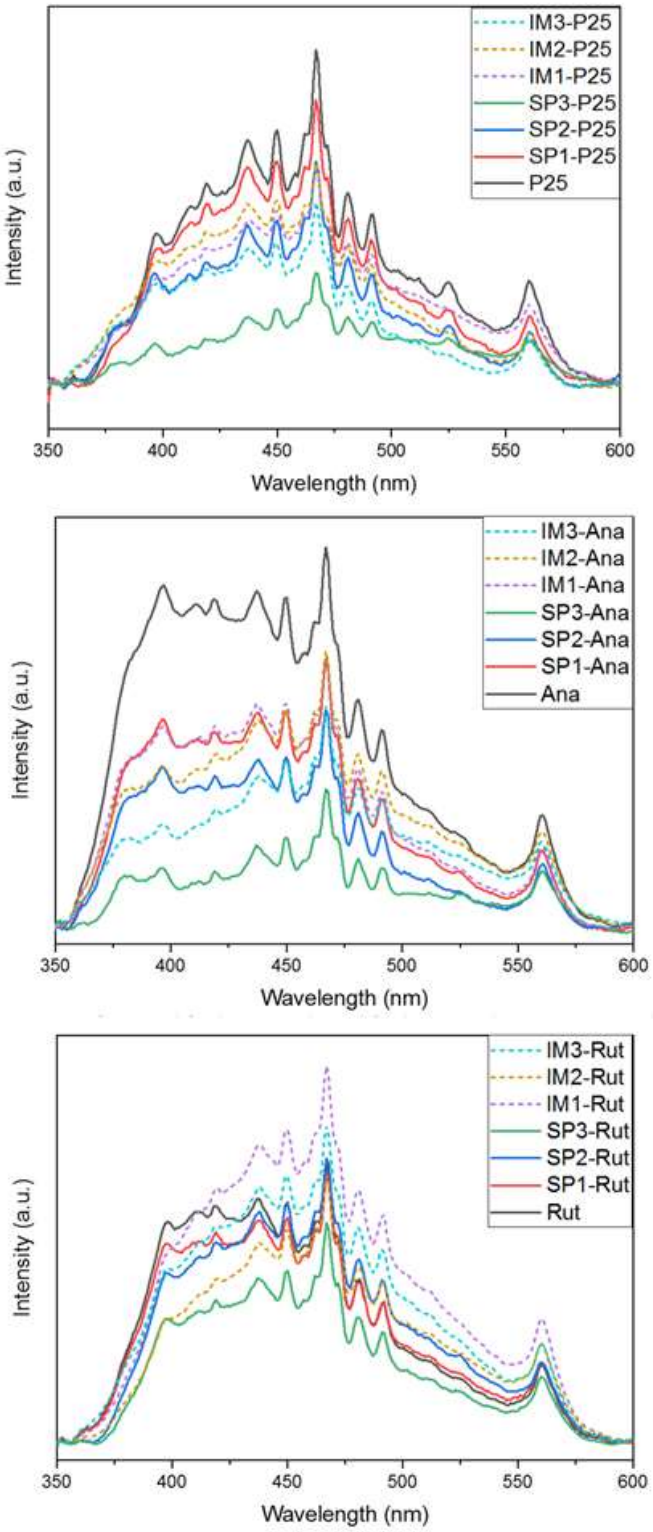

Figure 5. PL spectra of P25-TiO2, Ana-TiO_2 and Rut-TiO_2 modified Cu nanoparticles prepared by magnetron sputtering method and incipient wetness impregnation.

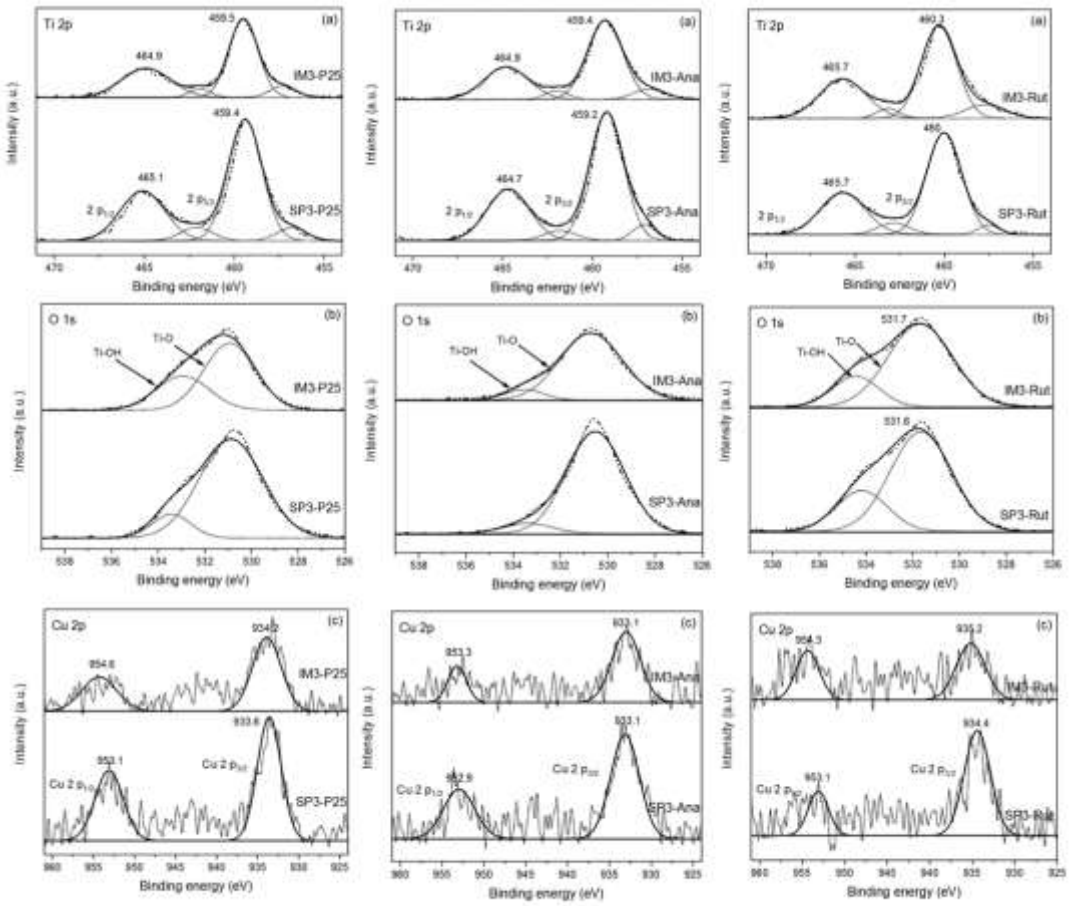

Figure 6. XPS spectra of Ti 2p, O 1s and Cu 2p of P25-TiO2, Ana-TiO_2 and Rut-TiO_2 modified Cu nanoparticles prepared by magnetron sputtering method and incipient wetness impregnation.

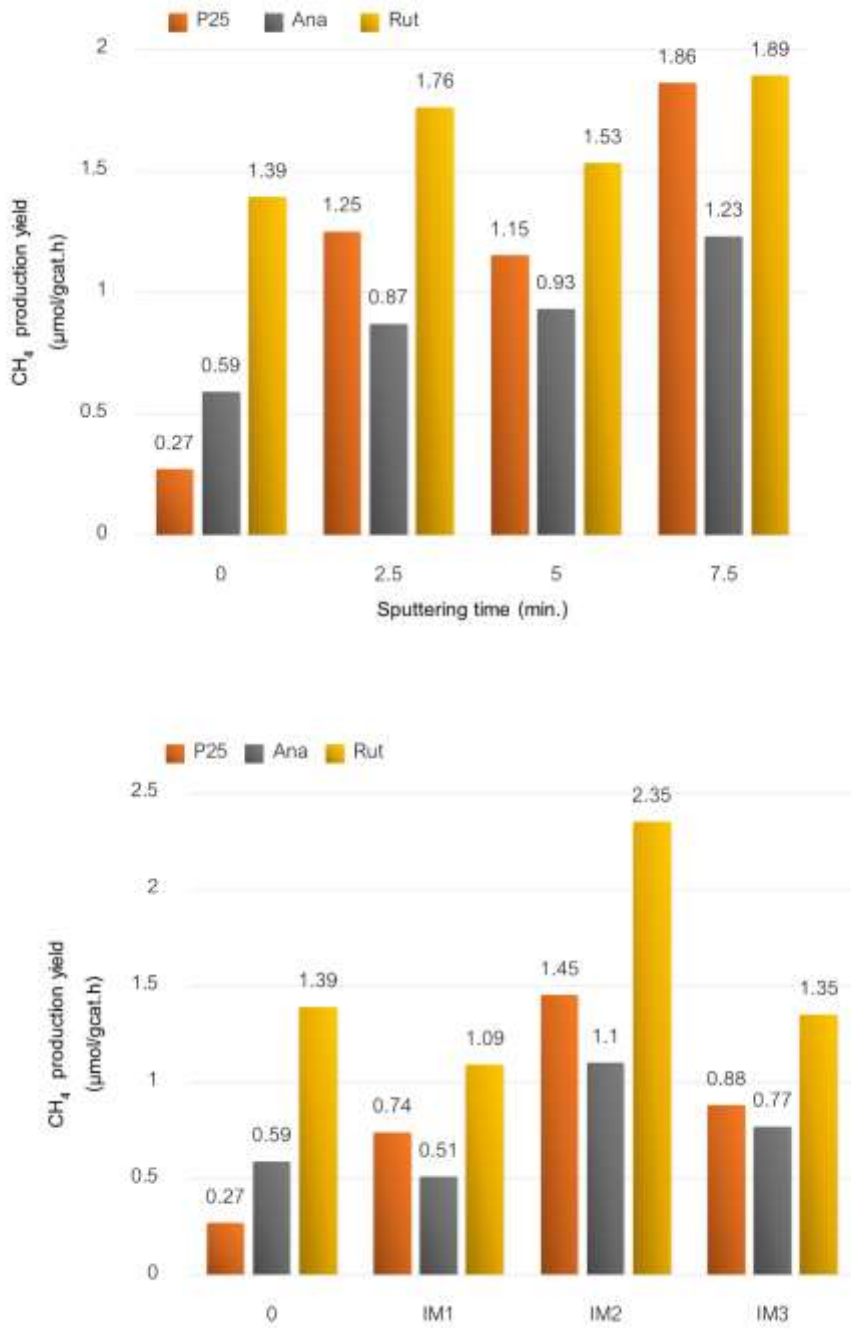

Figure 7. Comparison of CH_4 production yield of P25-TiO_2, Ana-TiO_2 and Rut-TiO_2 modified with Cu prepared by magnetron sputtering and incipient wetness impregnation methods.

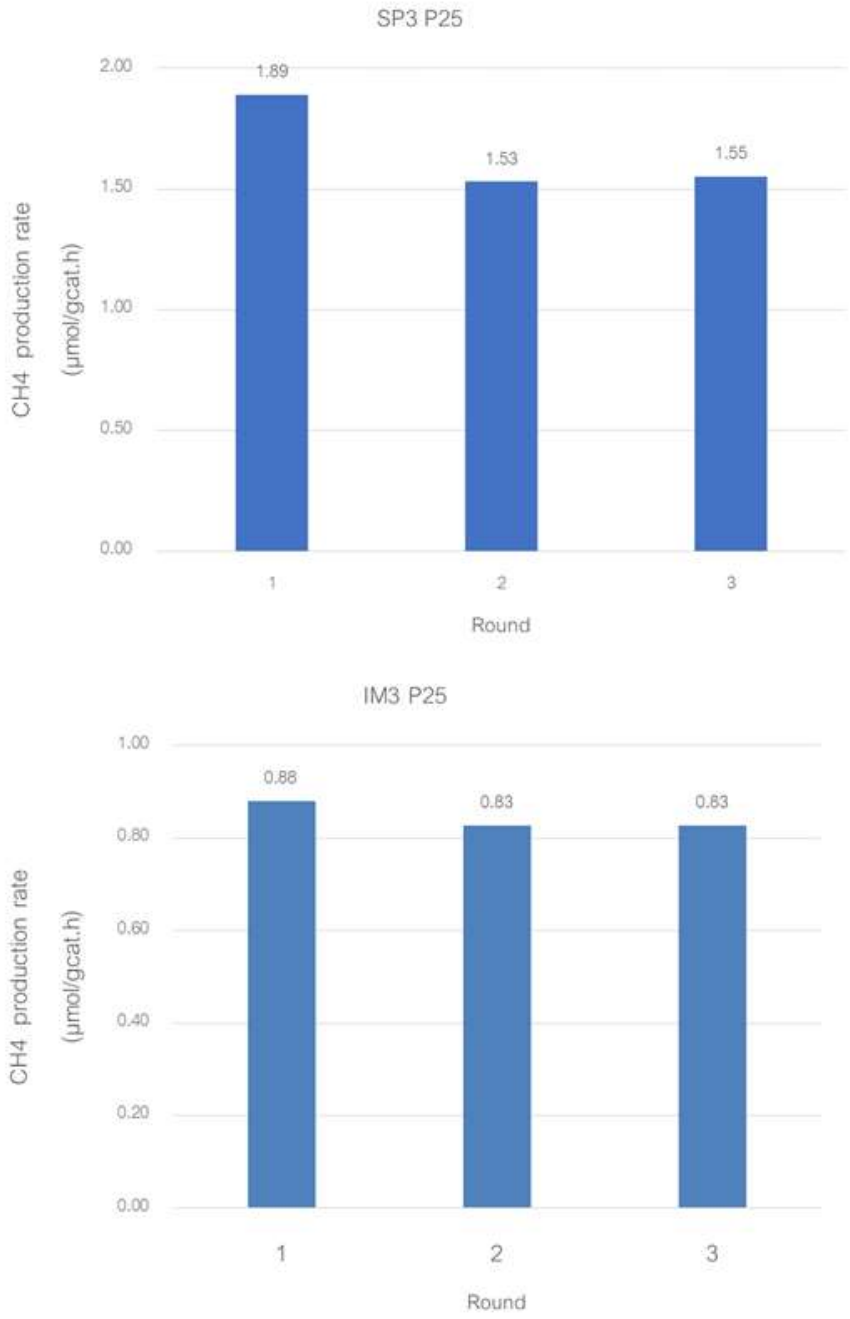

Figure 8. The catalytic performance of Cu deposited on P25 prepared by magnetron sputtering and incipient wetness impregnation methods under UV light irradiated for 6h at different cycles